ИЗВЕСТИЯ
КРЫМСКОЙ
АСТРОФИЗИЧЕСКОЙ
ОБСЕРВАТОРИИ

Изв.Крымской Астрофиз.Обс. 100, 74–85 (2004)

УДК 523.9

Numerical 3D simulation of acoustic wave scattering by the sunspot

K.V. Parchevsky

Crimean Astrophysical Observatory, Nauchny, Crimea 98409, Ukraine

Поступила в редакцию 24 июля 2003 г.

Аннотация. Построена численная модель "солнцетрясения", наблюдавшегося спутником SOHO 6 июля 1996 г. В результате численного моделирования взаимодействия звуковых волн с солнечным пятном показано, что фронт рассеянной волны отстает от невозмущенного фронта. Амплитуда фронта увеличивается при прохождении через пятно, что подтверждается наблюдениями. Скорости поверхностной сейсмической волны лежат в диапазоне от 16.7 км/с вблизи источника возмущения до 58.3 км/с на расстоянии 30 000 км.

NUMERICAL 3D SIMULATION OF ACOUSTIC WAVE SCATTERING BY THE SUNSPOT, *by K.V. Parchevsky.* A numerical model of the sunquake is built. The sunquake was observed by SOHO spacecraft on 6 July 1996. Numerical simulation of interaction of acoustic waves with the sunspot shows that the scattered wavefront is delayed with respect to the unperturbed one. Amplitude of the wavefront is increased when propagating through the sunspot, which is confirmed by observations. Speed of the surface seismic wave is in range from 16.7 km/s near the source to 58.3 km/s at the distance 30 000 km.

Keywords: Sun, local helioseismology, acoustics, numerical simulation

1 Introduction

A success of helioseismology on global scales initiated investigation of reconstruction of solar interior on smaller scale (local helioseismology). There are several methods for investigation of the interaction of traveling acoustic waves with small perturbations to the background state. One of them is the time-distance approach. The key concept of this method is the notion of wave travel time. Propagation of the high-frequency acoustic waves in this approach is calculated with ray theory. But, on theoretical grounds, the ray approximation is invalid near the surface, where the pressure and density scales vary rapidly, and wave effects must be taken into account (Bogdan, 1997). One important consequence of wave effects is the following: the travel time is sensitive not only to the local medium properties along the ray path, but also to conditions in the surrounding medium as well. More over, the travel-time sensitivity kernels calculated in the Born approximation (the first approximation to the wave theory) have *zero value along the ray path* (Kosovichev et al., 2000). So, transition from the geometrical acoustic (ray) approximation to the wave theory is not reduced to simple broadening of the ray kernels. One of the important consequence is that the sensitivity along the ray path is not proportional to the inverse local sound speed, but may varies significantly especially near the surface (Stark, Nikolaev, 1993). In this situation realistic simulations of

interaction of traveled acoustic waves with medium inhomogeneity are extremely welcome. One dimensional calculations were made by Kosovichev and Duvall (1997). Two dimensional numerical simulations were performed by Jensen, Jacobsen, and Christensen-Dalsgaard (1999). In this work a numerical 3D simulation of scattering of acoustic waves on the sunsport is presented. Realistic physics was used during these calculations. Equation of state was calculated by interpolation of OPAL tables, radiation transport in diffusion approximation was taken into account as well.

2 Linearized Euler equations

Acoustics problems are governed by the following linearized equations:

$$\begin{cases} \dfrac{\partial \rho'}{\partial t} + \dfrac{\partial}{\partial x}(\rho_0 u') + \dfrac{\partial}{\partial y}(\rho_0 v') + \dfrac{\partial}{\partial z}(\rho_0 w') = 0, \\ \dfrac{\partial}{\partial t}(\rho_0 u') + \dfrac{1}{\gamma_0}\dfrac{\partial p'}{\partial x} = 0, \\ \dfrac{\partial}{\partial t}(\rho_0 v') + \dfrac{1}{\gamma_0}\dfrac{\partial p'}{\partial y} = 0, \\ \dfrac{\partial}{\partial t}(\rho_0 w') + \dfrac{1}{\gamma_0}\dfrac{\partial p'}{\partial z} = -\dfrac{\rho' g_0}{Fr^2}, \\ \dfrac{\partial E'}{\partial t} + \dfrac{\partial}{\partial x}\left\{u'\left(\dfrac{\rho_0\,\mathcal{E}_0}{\gamma_0(\gamma_0-1)} + \dfrac{p_0}{\gamma_0}\right) - \hat{K}\dfrac{T_0^3}{\rho_0}\dfrac{\partial T'}{\partial x}\right\} + \\ \qquad \dfrac{\partial}{\partial y}\left\{v'\left(\dfrac{\rho_0\,\mathcal{E}_0}{\gamma_0(\gamma_0-1)} + \dfrac{p_0}{\gamma_0}\right) - \hat{K}\dfrac{T_0^3}{\rho_0}\dfrac{\partial T'}{\partial y}\right\} + \\ \qquad \dfrac{\partial}{\partial z}\left\{w'\left(\dfrac{\rho_0\,\mathcal{E}_0}{\gamma_0(\gamma_0-1)} + \dfrac{p_0}{\gamma_0}\right) - \hat{K}\dfrac{T_0^3}{\rho_0}\left[\left(3\dfrac{T'}{T_0} - \dfrac{\rho'}{\rho_0}\right)\dfrac{\partial T_0}{\partial z} + \dfrac{\partial T'}{\partial z}\right]\right\} = \\ \qquad -\dfrac{\rho_0 g_0 w'}{Fr^2}, \\ E' = \dfrac{\rho'\,\mathcal{E}_0}{\gamma_0(\gamma_0-1)} + \rho_0\left[\dfrac{\mathcal{E}'}{\gamma_0(\gamma_0-1)} + \dfrac{1}{2}(u'^2 + v'^2 + w'^2)\right], \end{cases} \tag{1}$$

where $\rho', p', T', E', \mathcal{E}', u', v', w'$ are perturbations of the density, pressure, temperature, total energy, specific energy, and velocity components respectively, γ_0 represents specific heat c_p/c_v of the reference model on the top boundary. Values in the reference state are denoted by zero subscript. The standard solar model is chosen as a reference state. Radiation transport in diffusion approximation is taken into account. Realistic equation of state is calculated using OPAL tables. Equations (1) are written in dimensionless variables in units of corresponding variables on the top boundary of the reference state. Dimensionless parameters

$$Fr^2 = \frac{\hat{a}_0^2}{\hat{g}_0 L}, \qquad \hat{K} = \frac{4ac}{3\kappa}\frac{\hat{T}_0^4}{\hat{a}_0^3 \hat{\rho}_0^2 L} \tag{2}$$

represent squared Froude number and dimensionless inverse opacity respectively. Hat denotes values in the reference state on the top boundary. Here c is the light speed, $a = 8\pi^5 k^4/15c^3h^3$ is the radiation constant, κ is the opacity, $\hat{a}_0^2 = \gamma_0 \hat{p}_0/\hat{\rho}_0$ is the squared sound speed in the reference model on the top boundary.

As far as we study small perturbations of the reference state, we can use the following procedure for calculation of perturbations of thermodynamic variables without direct access to OPAL tables. Thermodynamic quantities $p_0, \rho_0, T_0, \mathcal{E}_0$, known from the reference model, are linked by the realistic equation of state, which can be calculated by interpolation of OPAL tables. Assume, that the gas is locally perfect

$$p = R^* \rho T, \qquad \mathcal{E} = \frac{R^* T}{\gamma - 1}, \tag{3}$$

where R^* is the local gas constant which is changed from point to point. Hence for given quantities $p_0, \rho_0, T_0, \mathcal{E}_0$ one can calculate local values

$$\left(\frac{R^*}{\gamma-1}\right)_0 = \frac{\mathcal{E}_0}{T_0}, \qquad R_0^* = \frac{p_0}{\rho_0 T_0}. \tag{4}$$

Assume, that for calculation of perturbed values $\mathcal{E}_0 + \mathcal{E}'$ and $T_0 + T'$ we can use the same constants

$$\mathcal{E}_0 + \mathcal{E}' = \left(\frac{R^*}{\gamma-1}\right)_0 (T_0 + T'), \qquad \mathcal{E}' = \frac{\mathcal{E}_0}{T_0} T', \tag{5}$$

$$p_0 + p' = R_0^*(\rho_0 + \rho')(T_0 + T'), \qquad p' = \frac{p_0}{\rho_0 T_0}(\rho_0 T' + \rho' T_0). \tag{6}$$

3 Numerical scheme

One can write linearized Euler equations (1) in divirgent form

$$\frac{\partial \mathbf{q}}{\partial t} + \frac{\partial \mathbf{F}}{\partial x} + \frac{\partial \mathbf{G}}{\partial y} + \frac{\partial \mathbf{H}}{\partial z} = \mathbf{S}, \tag{7}$$

where $\mathbf{q} = (\rho', \rho_0 u', \rho_0 v', \rho_0 w', E')^T$ is the vector of independent variables. Vectors $\mathbf{F}$, $\mathbf{G}$, $\mathbf{H}$, and $\mathbf{S}$ can be easily obtained from (1). Following Tam and Webb (1993), we generalized this approach for 3D. A high-order four-level finite difference scheme was chosen to solve this system. A special choice of approximation of spatial and time derivatives permits us to preserve dispersion relations. Details of this technique will be discussed in the next section.

$$\mathbf{q}_{i,k,j}^{(n+1)} = \mathbf{q}_{i,k,j}^{(n)} + \Delta t \sum_{m=0}^{3} b_m \mathbf{K}_{i,k,j}^{(n-m)}, \tag{8}$$

$$\mathbf{K}_{i,k,j}^{(n)} = -\frac{1}{\Delta x}\sum_{m=-3}^{3} a_m \mathbf{F}_{i,k,j+m}^{(n)} - \frac{1}{\Delta y}\sum_{m=-3}^{3} a_m \mathbf{G}_{i,k+m,j}^{(n)} - \frac{1}{\Delta z}\sum_{m=-3}^{3} a_m \mathbf{H}_{i+m,k,j}^{(n)} + \mathbf{S}_{i,k,j}^{(n)}, \tag{9}$$

where i, k, j are the indices of the z, y and x mesh points respectively, n is the time level. If $\mathbf{q} = \mathbf{q}_{initial}$ at $t = 0$ is the initial conditions for the Euler equations (1), the appropriate initial conditions for the finite difference scheme can be choosen in the following way:

$$\mathbf{q}_{i,k,j}^{(n)} = \begin{cases} \mathbf{q}_{i,k,j}^{(n)} = \mathbf{q}_{initial} & \text{if } n = 0 \\ \mathbf{q}_{i,k,j}^{(n)} = 0 & \text{if } n < 0 \end{cases} \tag{10}$$

Zero boundary conditions were imposed at the edges of computational domain. Stability analysis shows that proposed scheme is stable if time step Δt smaller than

$$\Delta t_{max} = \frac{\Delta z}{a_0} \frac{0.4}{1.75\left[\frac{u_0}{a_0} + \sqrt{1 + \left(\frac{\Delta x}{\Delta z}\right)^2 + \left(\frac{\Delta y}{\Delta z}\right)^2}\right]}, \tag{11}$$

where u_0 is the velocity of the mean flow in the reference state, a_0 is the sound speed. In our case when the reference state is static $u_0 = 0$ and $\Delta x = \Delta y = \Delta z$ this expression reduces to

$$\Delta t_{max} = \frac{\Delta z}{a_0} \frac{0.4}{1.75\sqrt{3}}. \tag{12}$$

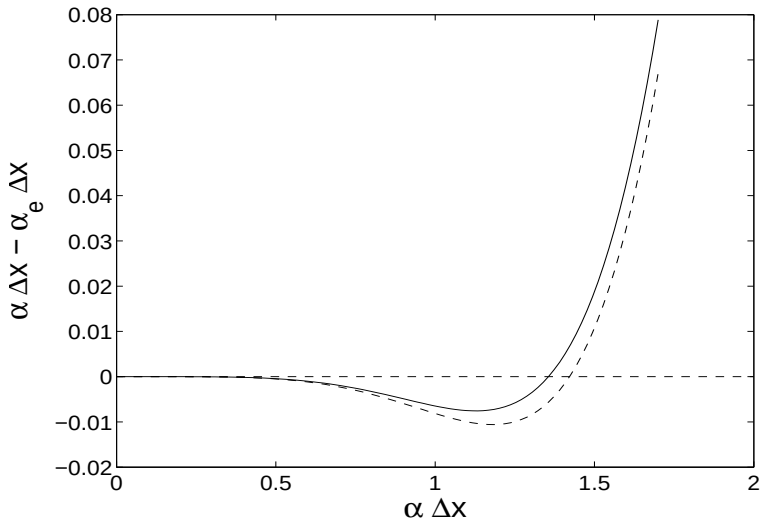

Fig. 1. Approximation error $\alpha\Delta x - \alpha_e\Delta x$ of spatial derivative in the Fourier space for two sets of a_j obtained analytically (solid line) and numerically (dashed line). Set of coefficients obtained analytically provides better approximation of spatial derivative for short waves

Damping analysis shows that the time step Δt must meet the numerical damping criterion $\Delta t \leq \Delta t_{damp}$ to prevent numerical damping, where expression for Δt_{damp} is given by (11) with the numenator equals 0.19 instead of 0.4. Numerical damping criterion is a more stringent criterion than that required for numerical stability. In other words to avoid excessive numerical dumping we have to choose time step approximately twice smaller than needed for numerical stability.

4 Derivative approximation

A high order dispersion-relation-preserving finite difference scheme was used to preserve properties of acoustic waves of high frequency. In usual high order finite difference schemes the first spatial derivative in the l-th node is approximated in the following way

$$\left(\frac{\partial f}{\partial x}\right)_l \simeq \frac{1}{\Delta x}\sum_{j=-3}^{3} a_j f_{l+j}, \tag{13}$$

where coefficients a_j are determined by expanding the right-hand side of (13) in Taylor series of Δx end equating coefficients of the same powers of Δx. In dispersion-relation-preserving finite difference scheme the coefficients are chosen in a different way to minimize the error of Fourier transform of the first spatial derivative. In other words, this scheme approximates the partial derivative in wave number space and gives better approximation of short length acoustic waves than usual Taylor series expansion. Taking Fourier transform of the left and right hand side of Eq.(13), one can obtain

$$i\alpha\tilde{f} \simeq \frac{\tilde{f}}{\Delta x}\sum_{m=-3}^{3} a_m e^{im\alpha\Delta x}, \tag{14}$$

where $\tilde{}$ represents the Fourier transform. Quantity

$$\alpha_e = -\frac{i}{\Delta x}\sum_{m=-3}^{3} a_m e^{im\alpha\Delta x} \tag{15}$$

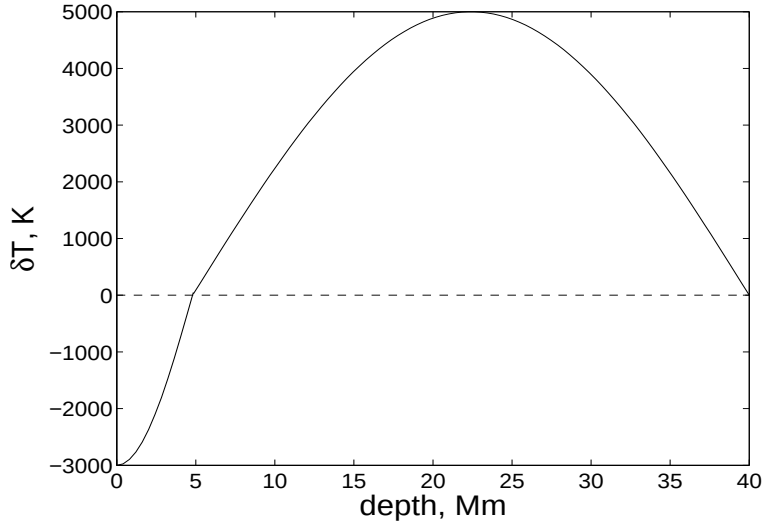

Fig. 2. Temperature variations $\delta T = T_{spot} - T_0$ in sunspot with respect to the reference model T_0

represents the effective wavenumber of Fourier transform of finite difference scheme (13). Effective wavenumber α_e is real if we use a symmetrical stencil for finite difference approximation of spatial derivative. In this case the right hand side of Eq.(15) is a truncated Fourier series. To assure that the Fourier transform of the finite difference scheme is a good approximation of the partial derivative in desired range of wave numbers it is required that a_j be chosen to minimize the integral error E_x, defined as

$$E_x = \int\limits_{-\pi/2}^{\pi/2} |\alpha\Delta x - \alpha_e \Delta x|^2 \, d(\alpha\Delta x). \tag{16}$$

To find a minimum of the integral error E_x, a solution of the following system

$$\frac{\partial E_x}{\partial a_j} = 0, \quad j = -3, ..., 3 \tag{17}$$

must be found. It is possible to combine the traditional truncated Taylor series and wave number approximation. We use 7-points central difference scheme. Assumtion that (13) must be accurate to order $(\Delta x)^4$ leaves two coefficient, say a_1 and a_{-1}, as free parameters, which can be found from minimization of integral error (16). It is straightforward to find an analytical solution for symmetrical $-3 \div 3$ stencil

$$\begin{cases} a_0 = 0 \\ a_{\pm 1} = \mp \dfrac{12}{15\pi - 32} \\ a_{\pm 2} = \pm \dfrac{96 - 27\pi}{128 - 60\pi} \\ a_{\pm 3} = \mp \dfrac{20 - 6\pi}{45\pi - 96} \end{cases} \tag{18}$$

We have found an analytical solution to Eq.(17). It gives better approximation of Fourier transform (14) than the set of numerically computed coefficients proposed in (Tam, Webb, 1993). Error $\alpha\Delta x - \alpha_e \Delta x$ of Fourier transform versus $\alpha\Delta x$ for these two cases is illustrated on Fig.1. The dashed curve represents the Fourier transform error for set of coefficients proposed in (Tam, Webb, 1993). The solid curve shows error

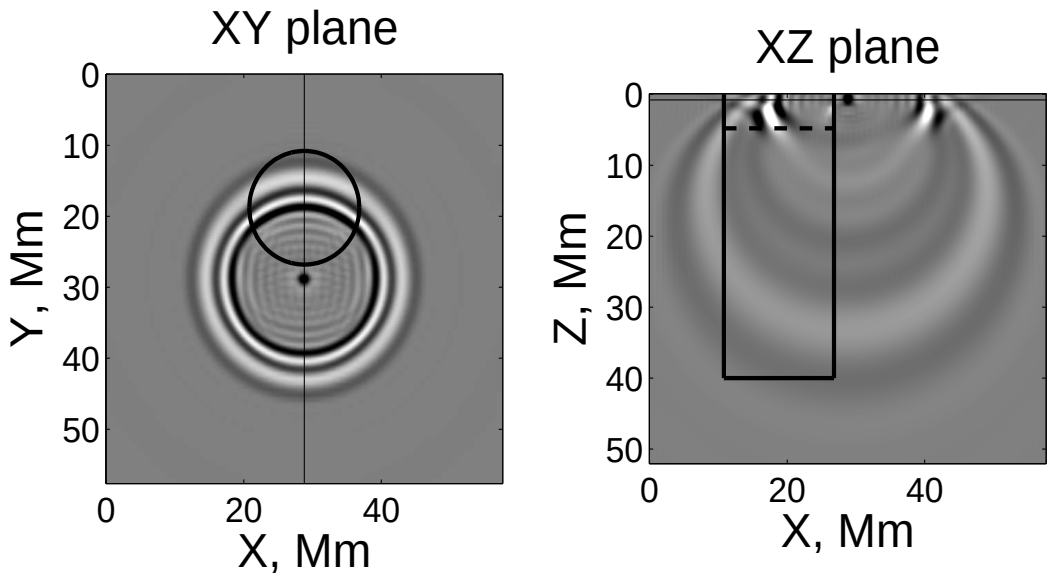

Fig. 3. Scattering of acoustic waves from the single pressure pulse on the sunspot at the moment $t = 151.4$ min. Brightness denotes density perturbation. Circle (on the left) and rectangle (on the right) drawn by thick lines show projections of the sunspot

for analytically obtained set of coefficients a_j. It is clear that the set of coefficients obtained analytically provides better approximation of spatial derivative for short waves.

On the boundaries we are forced to use a non-symmetrical stencil. Similar analytical solutions for a_j can be found in the case of non-symmetrical stencils. Explicit formulas for the coefficients of non-symmetrical stencils are written out in Appendix A.

Similar expressions can be obtained for approximation of time derivative

$$\mathbf{q}^{(n+1)} - \mathbf{q}^{(n)} \simeq \Delta t \sum_{j=0}^{3} b_j \left(\frac{d\mathbf{q}}{dt}\right)^{(n-j)}. \tag{19}$$

Three of four coefficients b_j for $j = 1, 2, 3$ are chosen so that (19) is satisfied to order $(\Delta t)^3$:

$$\begin{cases} b_1 = -3b_0 + \dfrac{53}{12}, \\ b_2 = 3b_0 - \dfrac{16}{3}, \\ b_3 = -b_0 + \dfrac{23}{12}. \end{cases} \tag{20}$$

The remaining coefficient b_0 is determined by the requiring that the Laplace transform of the finite difference scheme (20) be a good approximation of that of partial derivative. Taking Laplace transform of the left and right hand side of Eq. (20), one can obtain

$$-i\frac{i\left(e^{-i\omega\Delta t} - 1\right)}{\Delta t \sum_{m=0}^{3} b_m e^{im\omega\Delta t}} \tilde{\mathbf{q}} \simeq -i\omega\tilde{\mathbf{q}}, \tag{21}$$

where $\tilde{}$ represents the Laplace transform. Quantity

$$\omega_e = \frac{i\left(e^{-i\omega\Delta t} - 1\right)}{\Delta t \sum_{m=0}^{3} b_m e^{im\omega\Delta t}} \tag{22}$$

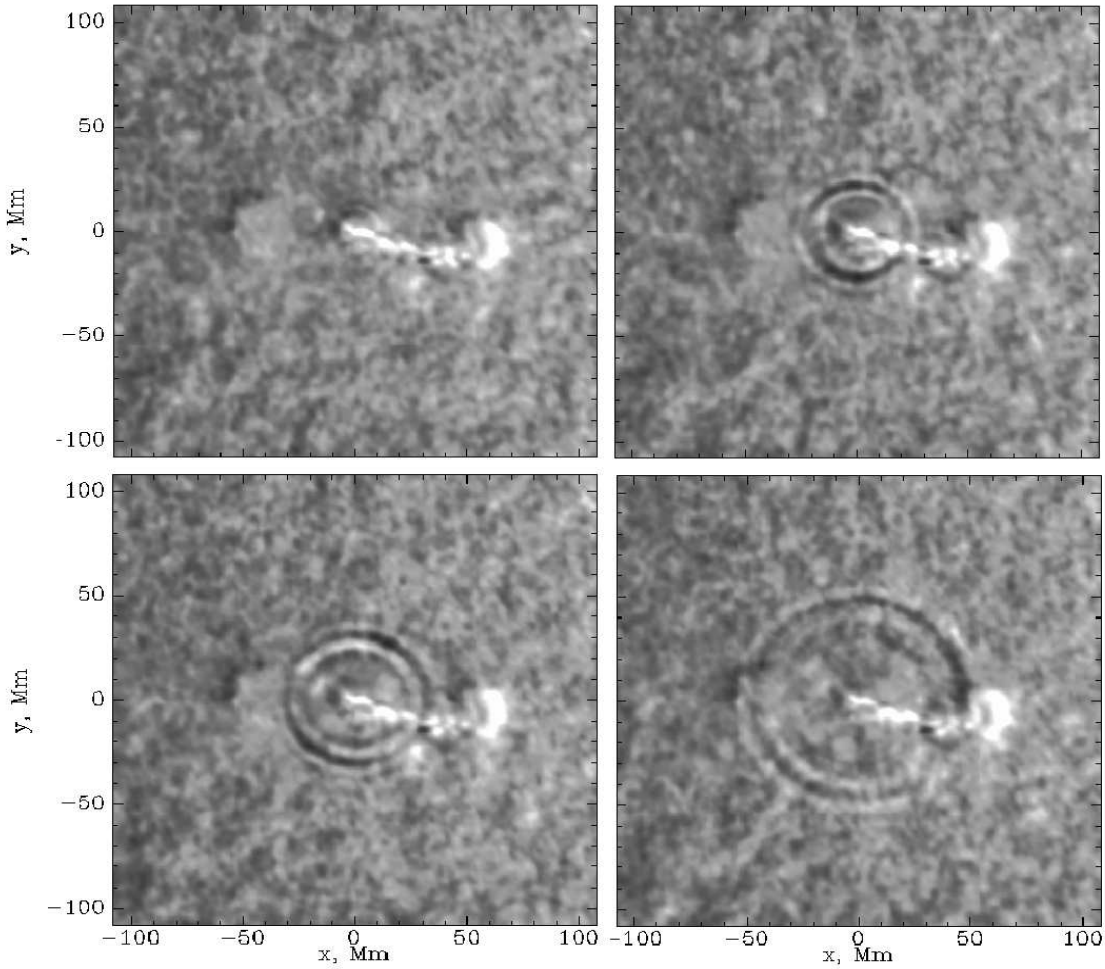

Fig. 4. A series of four snapshots of the "sunquake" observed by SOHO spacecraft on 6 July 1996. Amplitude of the perturbed wavefront is increased when the wave propagates through the sunspot

represents the effective angular frequency of the Laplace transform of Eq. (19). To assure that the Laplace transform of the finite difference scheme is a good approximation of the partial derivative the weghted integral error

$$E_t = \int_{-1/2}^{1/2} \left\{\sigma[\mathrm{Re}(\omega_e \Delta t - \omega \Delta t)]^2 + (1-\sigma)[\mathrm{Im}(\omega_e \Delta t - \omega \Delta t))]^2\right\} d(\omega \Delta t) \tag{23}$$

must be minimized by appropriate choosing of b_0. Here σ is the weight of real part. Coefficient b_0 can be found as the root of the equation

$$\frac{dE_t}{db_0} = 0. \tag{24}$$

The weight $\sigma \in [0,1]$ in Eq.(23) permits us to obtain either better wave propagation characteristics (real part of ω) for $\sigma \to 1$, or damping characteristics (imaginary part of ω) for $\sigma \to 0$. A table of coefficients b_j for different values σ is presented in Appendix.

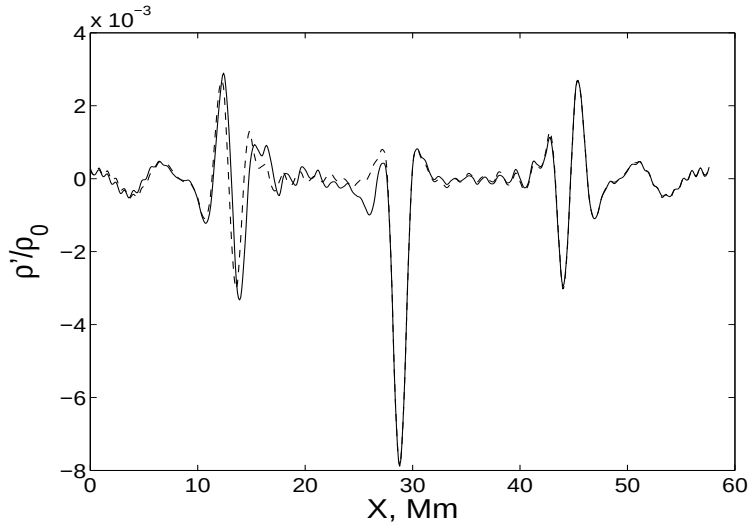

Fig. 5. Position of the wavefront after $t = 210.9$ min. The solid line represents a slice through the sunspot, the dashed one represents slice in the perpendicular direction

5 Results and discussion

3D version of algorithm discussed above was realized as a C++ program and applied for studying of acoustic wave propagation inside the Sun. Standard solar model was chosen as a reference state. The reference state is static i.e. we have neither rotation nor convection in the reference state. Thermodynamic quantities ρ_0, p_0, T_0, E_0 of the reference state are connected by realistic equation of state. To build the reference state we start from the density profile $\rho_0(r)$ which is taken from the standard solar model. Pressure profile is calculated from the condition of hydrostatic equilibrium

$$\frac{dp_0}{dr} = -\rho_0(r) g_0(r), \qquad g_0(r) = G\frac{4\pi \int_0^r \rho_0(r')\, dr'}{r^2}, \tag{25}$$

where G is the gravitational constant, $g_0(r)$ is the gravitational acceleration. When we know p_0 and ρ_0 we can calculate T_0 and $\mathcal{E}_0$ from equation of state, by interpolation of the OPAL tables.

We studied propagation of acoustic waves from a single pressure pulse located near the surface of the computational domain, and wave scattering on the sunspot. Sunspot was approximated by the cylinder with diameter $D = 16$ Mm and depth $H = 40$ Mm. To start simulation we have to know density, pressure, and temperature profiles in the sunspot. We define the temperature profile inside the sunspot by hands Fig. 2. There is temperature inversion on the depth 4.8 Mm. We use the following iterative procedure to obtain pressure and density profiles. As a zero order approximation we choose the density profile $\rho^{(0)} = \rho_0$ of the standard solar model and calculate $p^{(0)}$ from the condition of hydrostatic equilibrium. Using realistic OPAL equation of state we can calculate the first approximation for density: $(T_{spot}, p^{(0)}) \overset{\text{OPAL}}{\rightarrow} \rho^{(1)}$. We repeat this procedure until $\rho^{(n+1)}$ and $\rho^{(n)}$ become sufficiently close each other.

Rectangular computational domain $57.6 \times 57.6 \times 52.0$ Mm is covered by uniform grid $144 \times 144 \times 130$ with the step size $\Delta x = \Delta y = \Delta z = 400$ km. Time step must be chosen in accordance with the limitation (12). Maximum sound speed $a_0 = 97.5$ km/s is on the bottom boundary, hence $\Delta t_{max} = 0.54$ s. As an initial condition a single spherically symmetric gaussian pressure pulse was chosen. It was placed near the surface of the computational domain at the depth $H_{pulse} = 800$ km. Zero boundary conditions were imposed on all boundaries. A snapshot of the computational domain after $t = 151.4$ min is shown on Fig. 3. Brightness denotes the density perturbation. The left picture represents a horizontal XY-slice of the computational domain at the depth $z = 800$ km. The projection of this slice on the XZ plane is shown

on the right picture by the thin horizontal line near the surface. The right picture represents a vertical XZ-slice. Projection of this slice on the XY plane is shown on the left picture by the thin vertical line. Thick circle on the left and thick rectangle on the right represent projections of the sunspot. Horizontal dashed line on the right picture shows a position of temperature inversion level in the sunspot. Simulation was interrupted shortly after moment $t = 210$ min, because the reflection of acoustic waves from zero boundary conditions deteriorates the wave pattern completely. Results of series numerical simulations of acoustic wave scattering are presented as movies on the site

http://quake.stanford.edu/~pkv/HEPL/Seismology/

Pulse.mpg (wave propagation without sunspot),

Spot_R4Mm.mpg (acoustic wave scattering on the sunspot with $R = 4$ Mm),

Spot_R8Mm.mpg (acoustic wave scattering on the sunspot with $R = 8$ Mm).

These calculations represent a numerical model of the "sunquake" observed by SOHO on 6 July 1996. A series of four snapshots of the "sunquake" is shown on Fig. 4. One can see that the amplitude of the wave is increased when it propagates trough the small sunspot on the lower right snapshot.

Calculation of time delay of scattered wavefront is a problem of great interest. Results can be used in helioseismology for reconstruction of solar internal structure using time distance technique. Position of the wave front from single pressure pulse after $t = 210.9$ min is shown on Fig.5. The dashed line represents a slice of the left picture on Fig.3 in horizontal direction. It is clear that this curve have to be approximately symmetrical, because these parts of the wave front are not perturbed by the sunspot. It is interesting to compare this curve with the perpendicular slice which goes through the sunspot (solid line). The right part of this wavefront does not perturbed by the sunspot and almost coincide with the dashed curve. The left part of the wavefront perturbed by the sunspot is delayed in comparison with unperturbed part. Amplitude of the perturbed wavefront is increased when the wave propagates through the sunspot, which is confirmed by observations.

The time-distance diagram for the depth $h = 800$ km is shown on Fig. 6. Brightness denotes the density perturbation on the vertical slice of the left picture on Fig. 3. The slice goes through the sunspot. Its position is marked by the vertical solid line. It is important to emphasize that the lowest ridge corresponding to the surface seismic wave turns down while the wave front moves away from the source. Slope of the ridge determines a horizontal speed which increases from 16.7 km/s near the source to 58.3 km/s at the distance 30 000 km. Increasing of the surface wave speed is confirmed by SOHO observations.

Acknowledgements. Author thanks Prof. Phil Scherrer for invitation author to HEPL of Stanford University as a visiting scientist for three months that gave possibility to fulfil this work. Author thanks Dr. Alexander Kosovichev (scientific advisor) for statement of the problem, fruitful discussions and valuable remarks, and also for providing everything one can wish for productive work.

6 Appendix

Here we write out formulas for coefficients of non-symmetrical stencils used for approximation of spatial derivatives on the boundaries of the computational domain.

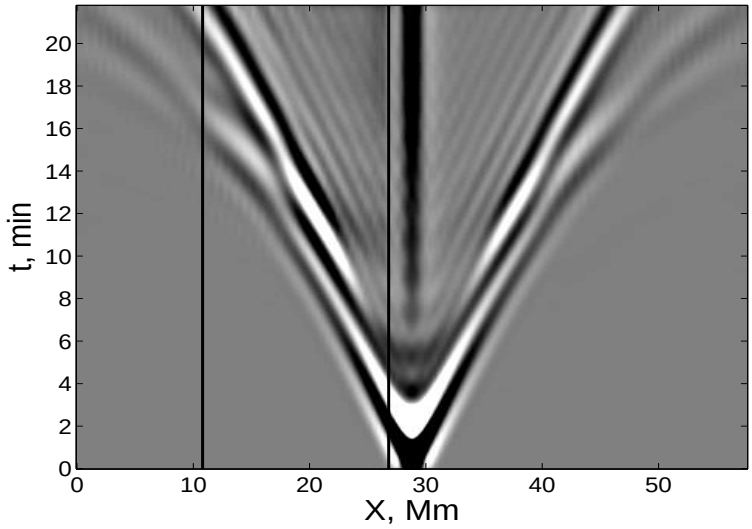

Fig. 6. Time distance diagram of the density perturbation on the depth $h = 800$ km. Position of the sunspot is shown by the vertical solid lines

$-4 \div 2$ stencil:

$$\begin{cases} a_0 = \dfrac{7}{12} - \dfrac{5}{15\pi - 56} - \dfrac{3}{30\pi - 88} \\ a_1 = \dfrac{4}{56 - 15\pi} \\ a_{-1} = \dfrac{4}{44 - 15\pi} \\ a_2 = \dfrac{1}{10} + \dfrac{1}{440 - 150\pi} - \dfrac{1}{56 - 15\pi} \\ a_{-2} = -\dfrac{3}{2} + \dfrac{5}{56 - 15\pi} - \dfrac{9}{88 - 30\pi} \\ a_{-3} = \dfrac{4}{15}\left(4 + \dfrac{9}{44 - 15\pi} - \dfrac{15}{56 - 15\pi}\right) \\ a_{-4} = -\dfrac{1}{4} + \dfrac{1}{56 - 15\pi} - \dfrac{1}{88 - 30\pi} \end{cases} \tag{26}$$

$-5 \div 1$ stencil:

$$\begin{cases} a_0 = \dfrac{46592 - 9\pi(2944 - 385\pi)}{12(6656 - 45\pi(64 - 5\pi))} \\ a_1 = \dfrac{1664 - 540\pi}{6656 - 45\pi(64 - 5\pi)} \\ a_{-1} = -\dfrac{1664 - 660\pi}{6656 - 45\pi(64 - 5\pi)} \\ a_{-2} = -5 + \dfrac{19968 - 6720\pi}{6656 - 45\pi(64 - 5\pi)} \\ a_{-3} = \dfrac{20}{3} - \dfrac{28288 - 9420\pi}{6656 - 45\pi(64 - 5\pi)} \\ a_{-4} = -\dfrac{15}{4} + \dfrac{80(208 - 69\pi)}{6656 - 45\pi(64 - 5\pi)} \\ a_{-5} = \dfrac{4(416 - 3\pi(91 - 15\pi))}{6656 - 45\pi(64 - 5\pi)} \end{cases} \tag{27}$$

$-6 \div 0$ stencil:

$$\begin{cases} a_0 = \dfrac{336-59\pi}{256-60\pi} \\ a_{-1} = -\dfrac{44}{56-15\pi} \\ a_{-2} = -\dfrac{1}{2} + \dfrac{220}{56-15\pi} - \dfrac{316}{64-15\pi} \\ a_{-3} = \dfrac{8}{3}\left(-2 + \dfrac{316}{64-15\pi} - \dfrac{165}{56-15\pi}\right) \\ a_{-4} = \dfrac{39}{4} + \dfrac{440}{56-15\pi} - \dfrac{948}{64-15\pi} \\ a_{-5} = \dfrac{4}{5}\left(-8 + \dfrac{632}{64-15\pi} - \dfrac{275}{56-15\pi}\right) \\ a_{-6} = \dfrac{3}{2} + \dfrac{44}{56-15\pi} - \dfrac{316}{3(64-15\pi)} \end{cases} \tag{28}$$

σ	b_0	b_1	b_2	b_3
0.00	2.45081168	–2.93576836	2.01910170	–0.53414501
0.05	2.42695750	–2.86420582	1.94753916	–0.51029083
0.10	2.40418226	–2.79588012	1.87921345	–0.48751559
0.15	2.38248172	–2.73077849	1.81411182	–0.46581505
0.20	2.36183980	–2.66885273	1.75218606	–0.44517313
0.25	2.34223095	–2.61002619	1.69335953	–0.42556429
0.30	2.32362227	–2.55420014	1.63753347	–0.40695560
0.35	2.30597561	–2.50126015	1.58459349	–0.38930894
0.40	2.28924912	–2.45108071	1.53441404	–0.37258246
0.45	2.27339885	–2.40352988	1.48686321	–0.35673218
0.50	2.25837982	–2.35847280	1.44180613	–0.34171315
0.55	2.24414703	–2.31577442	1.39910776	–0.32748036
0.60	2.23065612	–2.27530171	1.35863504	–0.31398946
0.65	2.21786393	–2.23692512	1.32025845	–0.30119726
0.70	2.20572885	–2.20051990	1.28385323	–0.28906219
0.75	2.19421112	–2.16596669	1.24930003	–0.27754445
0.80	2.18327292	–2.13315210	1.21648543	–0.26660625
0.85	2.17287851	–2.10196886	1.18530219	–0.25621184
0.90	2.16299420	–2.07231594	1.15564927	–0.24632754
0.95	2.15358838	–2.04409848	1.12743181	–0.23692171
1.00	2.14463142	–2.01722761	1.10056094	–0.22796476

References

Bogdan T. J. // Astroph.J. 1997. V. 477. P. 475.
Kosovichev A. G., Duvall T. L. Jr., Scherrer P. // Solar Phys. 2000. V. 192. P. 159.
Tam C., Webb J. // J. Comput. Phys. 1993. V. 107. P. 262.
Stark P.B., Nikolaev D.I. // J. Geophys. Res. 1993. V. 98. P. 8095.
Kosovichev A.G., Duvall T.L.Jr. // Acoustic Tomography of Solar Convective Flows and Structures, SCORe'96: Solar Convection and Oscillations and their Relationship. Eds. F.P. Pijpers, J. Christensen-Dalsgaard, and C.S. Rosenthal, Kluwer Academic Publishers, Dordrecht, Holland, 1997. P. 241.

Jensen J.M., Jacobsen B.H., Christensen-Dalsgaard J. // Smooth versus Sharp Frechet Kernel in Time-Distance Helioseismology, preprint, 1999.